materials

MDPI

Article

Enhanced Photoelectrochemical Properties of Ti^{3+} Self-Doped Branched TiO_2 Nanorod Arrays with Visible Light Absorption

Jingyang Wang [1,*], Xiantao Wang [1], Jun Yan [1], Qi Tan [1], Guijie Liang [2], Shaohua Qu [1] and Zhicheng Zhong [2]

1 School of Physics and Electronic Engineering, Hubei University of Arts and Science, Xiangyang 441053, China; 1502060441@gmail.com (X.W.); 18827551096yj@gmail.com (J.Y.); tanqi9504@gmail.com (Q.T.); qushaohua@hbuas.edu.cn (S.Q.)

2 Hubei Key Laboratory of Low Dimensional Optoelectronic Materials and Devices, School of Physics and Electronic Engineering, Hubei University of Arts and Science, Xiangyang 441053, China; liangguijie@hbuas.edu.cn (G.L.); zhongzhicheng@hbuas.edu.cn (Z.Z.)

* Correspondence: wangjingyang@hbuas.edu.cn; Tel: +86-0710-3590-894

Received: 29 August 2018; Accepted: 18 September 2018; Published: 20 September 2018

Abstract: A novel Ti^{3+} self-doped branched rutile TiO_2 nanorod arrays (NRAs) was successfully grown on an F-doped tin oxide (FTO) transparent conductive glass by a combined hydrothermal and magnetron sputtering method. Surface morphology, structure, optical properties, and photoelectrochemical behavior of the branched TiO_2 NRAs are determined. Using TiO_2 nanoparticles (NPs) deposited on the top of the nanorods as seeds, TiO_2 nanobranches can easily grow on the top of the nanorods. Moreover, the Ti^{3+} defects in the TiO_2 NPs and associated oxygen vacancies, and the nanobranches expend the optical absorption edge of the TiO_2 NRAs from 400 nm to 510 nm. Branched TiO_2 NRAs exhibit excellent photoelectrochemical properties compared to the pure TiO_2 NRAs, as revealed by photoelectrochemical measurements. This enhanced photoelectrochemical properties is induced by the increased surface area and expanded optical absorption range. Due to their favorable characteristics, these novel branched TiO_2 NRAs will provide a new path to the fabrication of hierarchical nanostructured materials.

Keywords: branched TiO_2 nanorod arrays; Ti^{3+} self-doped; hydrothermal; magnetron sputtering; photoelectrochemical properties

1. Introduction

In the past few years, titanium oxide (TiO_2) nanoarrays (i.e., nanotube, nanorod, and nanowire (NW) arrays) have attracted considerable attention as photoelectrodes in various photoelectrochemical (PEC) applications [1–3]. Compared with conventional TiO_2 nanoparticle (NP)-film photoelectrodes, TiO_2 nanoarray photoelectrodes have direct and ordered carrier transport channels, which can decouple a minor amount of charge diffusion paths into different directions to improve charge collection efficiency [4,5]. Moreover, with vertically aligned one-dimensional (1D) structures, light scattering and absorption can be improved greatly [6].

Among these 1D TiO_2 nanoarrays, TiO_2 nanorod arrays (NRAs) have been recognized as one of the most anticipated TiO_2 nanoarrays due to unique physical and chemical properties and excellent stability [7,8]. Nevertheless, TiO_2 NRAs are limited to a small specific surface area and a wide band gap (3.2 eV). Many efforts have been made to overcome these limitations of TiO_2 NRAs. The growth of branched TiO_2 NRAs has been proven to be an effective way to increase the specific surface area [9–12]. Wang et al. [9] prepared branched rutile TiO_2 NRAs via a two-step wet chemical synthesis process, and Cho and co-workers [10] also prepared a kind of branched TiO_2 NRAs by a two-step hydrothermal

process by using a $TiCl_3$ aqueous solution as a precursor for the growth of branches. Similarly, flower-like branched TiO_2 NRAs have been prepared by Liu and co-workers with a modified two-step hydrothermal method [12]. It is found that the anatase/rutile junctions on the surface of TiO_2 nanorod are favorable to the photoelectric properties of NRAs. Nevertheless, these TiO_2 branches are still relatively short. Besides, many attempts such as element doping [13] and sensitization with dyes or narrow band-gap semiconductors [14,15] have been made to extend optical absorption ranges of TiO_2 NRAs. Unfortunately, the stability of these dyes and semiconductors is not satisfactory. Thus, at the present, it is still attractive to develop novel branched TiO_2 NRAs that exhibit a larger surface area and a wider absorption range at the same time. To the best of our knowledge, such attempts have been rarely reported.

In this paper, following our previous work on synthesis of branched TiO_2 NRAs and TiO_2 NP/NRA composites [16,17], a combined magnetron sputtering and hydrothermal method has been developed to grow Ti^{3+} self-doped branched TiO_2 NRAs. With the larger surface area and improved optical absorption, the PEC properties of branched TiO_2 NRAs are significantly improved compared with those of pure TiO_2 NRAs.

2. Materials and Methods

First, TiO_2 NRAs were prepared on TiO_2-seeded FTO transparent conductive glass using the typical hydrothermal method [17]. Half a milliliter titanium butoxide was added to a 24-mL de-ionized (DI) water and hydrochloric acid (mass fraction: 36.5–38%)-mixed solution (a volume ratio of DI water and hydrochloric acid is 1:1). The mixture was stirred for 10 minutes and transferred to a 50-mL Teflon lined stainless steel autoclave. A TiO_2-seeded FTO transparent conductive glass was put in the Teflon liner and heated to 150 °C for 5 h. After the growth of TiO_2 NRAs, Ti NPs were deposited on the top of the TiO_2 NRAs by direct current (DC) magnetron sputtering in a physical vapor deposition system (PVD75, Kurt J. Lesker Company, Jefferson Hills, PA, USA). A high-purity titanium wafer (99.995%, ZhongNuo Advanced Material Technology CO., LTD, Beijing, China) was used as a sputtering target. The base vacuum of the sputtering chamber was 1.0×10^{-6} Torr and the deposition pressure was carried out at 8 m Torr by using Ar gas (99.999%) as the working gas. The source-to-sample distance and the sample rotation speed were 150 mm and 6 rev·min^{-1}, respectively. The sputtering power was 100 W and maintained for 60 min. The substrate temperature was kept at room temperature. The prepared products were annealed in air at 450 °C for 1 h to form TiO_2 NP/NRA composites.

For the formation of branched TiO_2 NRAs, the prepared TiO_2 NP/NRA composites were subjected to a second hydrothermal treatment. DI water (12.5 mL), HCl (12.5 mL), and titanium butoxide (0.15 mL) were used as the precursor. The mixture was added into the autoclave, to which the TiO_2 NP/NRAs composite was placed in. The autoclave temperature was increased to 160 °C for 3 h. After the synthesis, the branched TiO_2 NRAs were rinsed with DI water and ethanol. The final annealing was performed at 450 °C for 30 min.

The phase structures of as-prepared products were identified by X-ray diffraction (XRD, D8 Advance, Bruker, Madison, WI, USA) with Cu-Kα radiation (λ = 1.54060 Å), and the 2θ scanning speed was 5°/min. The morphologies and microstructure were studied on a field-emission scanning electron microscope (FESEM, Hitachi, S-4800 and acceleration voltage was 10 kV, Tokyo, Japan). Transmission electron microscopy (TEM) and high-resolution TEM (HRTEM) images were obtained on an FEI Tecnai G2 F30 microscope operating at 200 KV, Hillsboro, OR, USA. X-ray photoelectron spectroscopy (XPS) was conducted on an ESCALAB 250Xi (Thermo, Waltham, MA, USA) system with an Al-*Kα* X-ray source. The spot size was 500 μm and the energy step size was 0.1 eV. Diffuse reflectance and absorption spectra were measured using a UV-Vis spectrophotometer (UV-3600, Shimadzu, Kyoto, Japan) equipped with integrating spheres with a scanning range of 300 nm to 700 nm by scanning at a high scan speed. The sample interval and slit width were 0.5 nm and 20 nm, respectively. PEC measurements and electrochemical impedance spectroscopy (EIS) were determined on an electrochemical workstation (Autolab/PGSTAT302N, Metrohm Autolab, Herisau; Switzerland) with a

standard three-electrode electrochemical cell in a 0.5-M Na_2SO_4 solution. TiO_2 NRAs, or branched TiO_2 NRAs were used as working electrodes; a platinum plate electrode (dimension: 15 mm × 15 mm) was used as the counter electrode and Ag/AgCl in saturated KCl as the reference electrode. A Xe lamp with an intensity of 100 W/cm^2 was used as the illumination source. The active area of the working electrode was 1.5 cm^2. The frequency range of EIS measurements was from 0.01 Hz to 100 kHz and the ac amplitude was set at 10 mV.

3. Results and Discussion

The morphologies of TiO_2 NRAs, TiO_2 NP/NRA composites, and branched TiO_2 NRAs are shown in Figure 1a–f. Figure 1a displays the surface SEM image of TiO_2 NRAs, exhibiting a unified rod-like structure. Figure 1b presents the side-view SEM image of the same sample, and its inset shows higher-magnification image of the arrays, exhibiting that the nanorods grew nearly vertically on the substrate with a length of about 2.5 μm. When Ti NPs were deposited on the top of TiO_2 NRAs and annealed to form TiO_2 NPs/NRAs composites, the initial square morphology of the nanorods changed to sphere morphology, as shown in Figure 1c,d. The match-like TiO_2 NP/NRA composites were then subjected to the second hydrothermal growth, and tree-like branched TiO_2 NRAs were formed successfully (see Figure 1e,f). It was noticed that the nanobranches densely and uniformly covered TiO_2 nanorods on the top. The length of nanobranches was much longer than those previously reported, which are grown on the side surface of TiO_2 nanorods [10–12]. Close observation (the inset in Figure 1f) shows that the branches mainly grew on the top of the nanorods and diverged in all directions to form a spherical shape. Obviously, these nanobranches significantly increased the surface area of the TiO_2 NRAs.

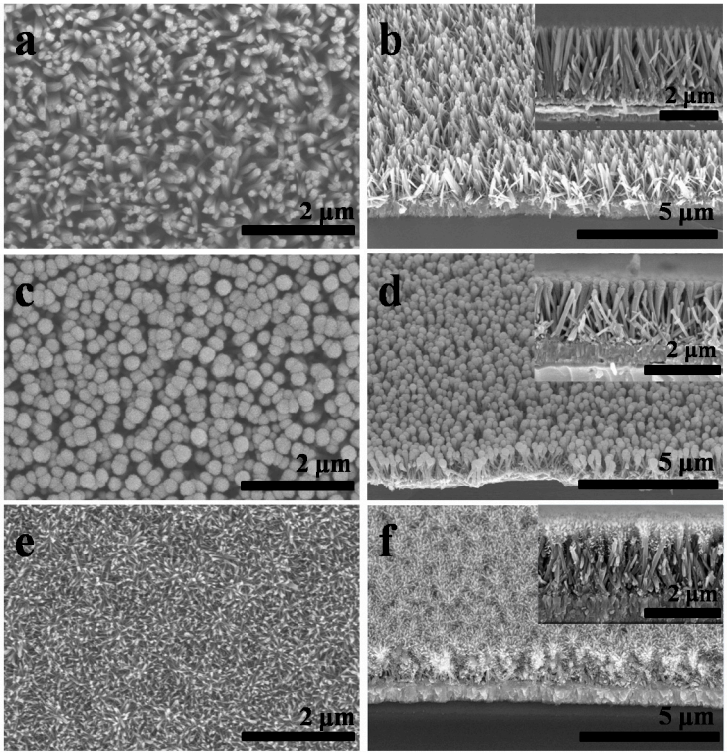

Figure 1. Surface and side-view SEM images of the TiO_2 NRAs (**a**,**b**); NPs/NRAs (**c**,**d**); and branched NRAs (**e**,**f**). The insets in b, d and f show high-magnification SEM images of TiO_2 NRAs, NPs/NRAs and branched NRAs, respectively.

Figure 2a shows the XRD patterns of TiO_2 NRAs, TiO_2 NP/NRA composites, and branched TiO_2 NRAs. The XRD patterns showed that all the crystal structures of these three samples could be classified as the tetragonal rutile phase of TiO_2. The peak intensities of the (101), (110), and (002) planes

of branched TiO_2 NRAs were stronger than those of pure NRAs. This indicated that the branches were well crystallized, and the growth mechanism is the same as for the TiO_2 nanorod trunk. The growth rate on the (101) plane of rutile TiO_2 nanorods is faster than that on the (110) plane [7,18], explaining the greatly enhanced intensity of the diffraction peak of the (101) plane with respect to the other diffraction peaks. Figure 2b shows the formation process of the branched TiO_2 NRA structure. The deposited TiO_2 NPs at the top of the nanorods served as crystal seeds for subsequent branching growth at energetically favorable sites on the top of nanorods. As shown in Figure 1f, TiO_2 seeds were grown into dendritic branches, while the nanorod trunks did not grow further.

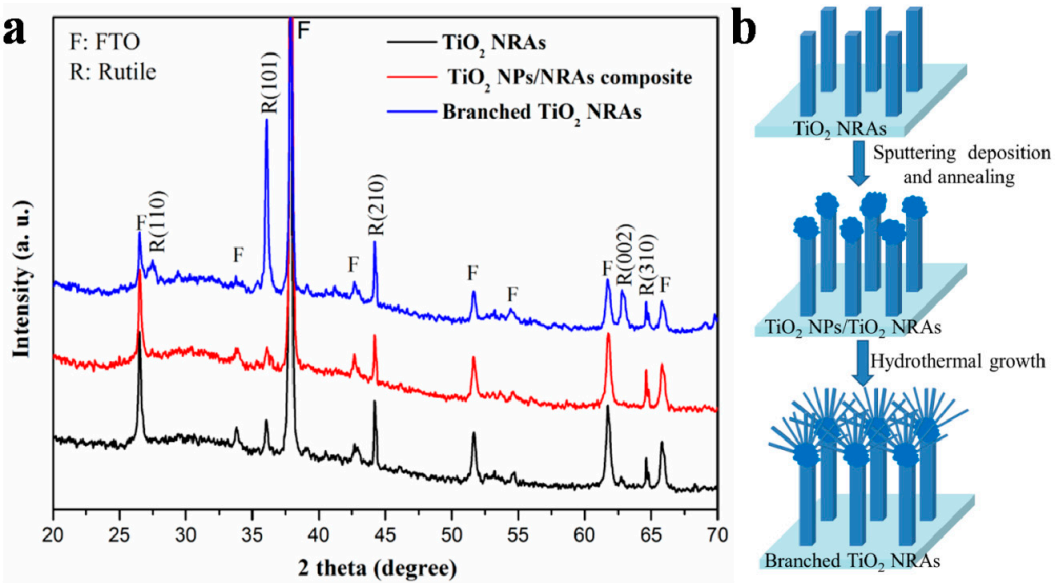

Figure 2. (**a**) XRD patterns of TiO_2 NRAs, Nps/NRAs and branched NRAs; and (**b**) schematic growth of branched TiO_2 NRAs.

Figure 3a displays the TEM image of branched TiO_2 NRAs. It can be seen that nanobranches with about 200 nm in length and 40 nm in diameter uniformly covered nanorods on the top. The HRTEM image of a single branch is shown in Figure 3b, which exhibited clear and discernible lattice fringes, indicating good crystallinity of TiO_2 nanobranches. The lattice constant with an interplanar spacing of 0.32 nm in the parallel direction to the length suggested the nanobranches were also crystallized to tetragonal rutile phase and had the same [001] growth direction as nanorods.

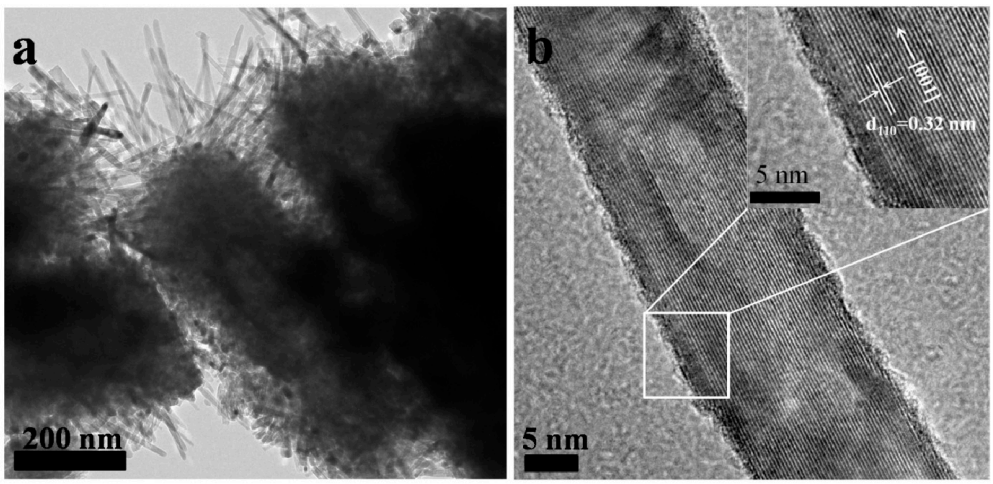

Figure 3. Overlapping of TEM and HRTEM images of (**a**) branched TiO_2 NRAs and (**b**) a single branch.

XPS was exploited to characterize the chemical valence state and composition of branched TiO_2 NRAs. As shown in Figure 4a, the observed two peaks at 458.6 and 464.4 eV corresponded to Ti $2p_{3/2}$ and Ti $2p_{1/2}$ of the branched TiO_2 NRAs, respectively. Two Ti 2p peaks can be deconvoluted into four peaks, including the peaks of Ti^{3+} $2p_{3/2}$ at 457.7 eV and Ti^{3+} $2p_{1/2}$ at 463.7 eV, which indicates the existence of Ti^{3+} species [19]. These Ti^{3+} species are introduced by TiO_2 NPs at the top of the nanorods [20–23]. In this case, the Ti NPs were deposited on the top of the nanorods by magnetron sputtering, and then annealed in air to form TiO_2 NPs, which can also form a certain amount of reduced TiO_2 (TiO_{2-x}) and result in the formation of Ti^{3+} species. On the other hand, in order to maintain the charge equilibrium, oxygen vacancies were formed around Ti^{3+} defects. The O 1s spectrum is shown in Figure 4b. The main peak at 529.9 eV can be assigned to the O lattice of TiO_2 and the binding energy of 531.3 eV can be ascribed to lattice oxygen (Ti–O) and oxygen in surface –OH groups [24]. Ti^{3+} defects and oxygen vacancies existing in the branched TiO_2 NRAs can cause the formation of TiO_2-localized states, thus promoting the separation of photoinduced electrons and holes [25,26].

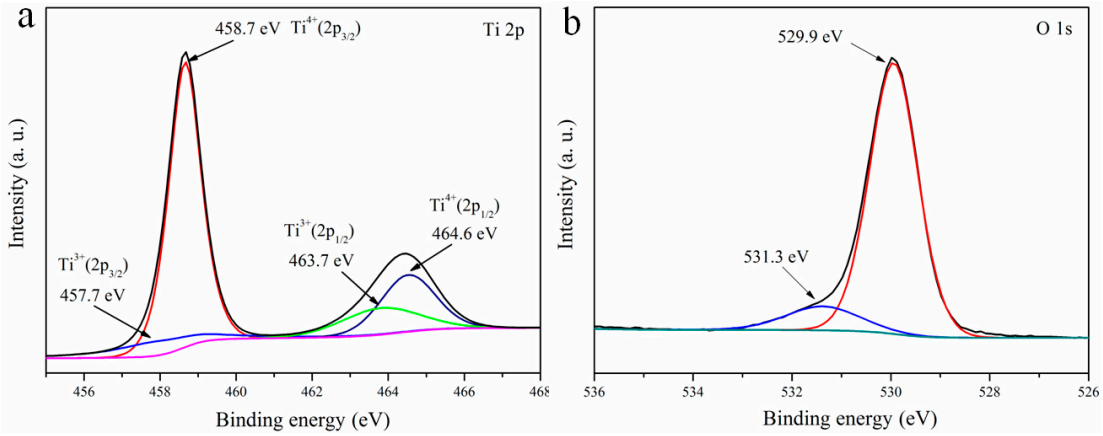

Figure 4. XPS spectra of the branched TiO_2 NRAs: (**a**) Ti 2p; (**b**) O 1s.

The light absorption properties of branched TiO_2 NRAs and pure TiO_2 NRAs were studied by diffuse reflection absorption spectroscopy. The rutile TiO_2 NRAs exhibited a single absorption edge at 400 nm, consisting with the rutile TiO_2 band gap of 3.0 eV. Distinct from the TiO_2 NRAs, the spectrum of the branched TiO_2 NRAs (Figure 5a) exhibited a structure of multiple band gaps, and a new absorption edge appeared around the 510 nm, which was a strong indicator for the unique geometric structure. The inset in Figure 5a shows the photographic images of TiO_2 NRAs and branched TiO_2 NRAs. The pure TiO_2 NRAs showed gray white color, while the branched NRAs changed to light yellow. Furthermore, a plot of the modified Kubelka–Munk function $[F(R\infty)E]^{1/2}$ vs. the energy of absorbed light E was used to calculate values of E_{gap1} and E_{gap2} to be 3.0 eV and 2.43 eV for these two band gaps, respectively, as shown in Figure 5b. The multiple band gaps presented in the branched NRAs should result from two reasons: (i) defect energy levels introduced by Ti^{3+} species in the reduced TiO_2 NPs at the top of the nanorods, which was confirmed by the XPS results. It has been demonstrated that reduced TiO_2 (TiO_{2-x}), which contains the Ti^{3+} or oxygen vacancy, exhibit visible light absorption [23–25]; (ii) the quantum confinement of the electrons in the TiO_2 nanobranches. Previous studies have demonstrated that, when the diameter of anatase TiO_2 NWs reduces to 40 nm, the multiple band-edge absorptions could occur, which can be induced by quantum confinement [27,28]. In this work, the morphology of TiO_2 nanobranches was similar to that of TiO_2 NWs, and the diameter of nanobranch was about 40 nm. Therefore, the absorption step could be also attributed to the quantum confinement in rutile TiO_2 nanobranches. Figure 5c presents the reflectance spectrum of the TiO_2 NRAs and branched NRAs. Obviously, branched TiO_2 NRAs exhibited lower reflectance as compared to the pure TiO_2 NRAs. The branched nanorod structure with higher surface roughness can increase the incident light scattering path, and result in the reflectivity reduction of branched NRAs [29,30].

However, it was also noticed that the branched TiO_2 NRAs had lower absorption than that of TiO_2 NRAs at the wavelength range from 510 nm to 700 nm even though the surface area increased, which can be ascribed to the light scattering effect from the increased surface roughness of the branched geometric structure [12,31,32].

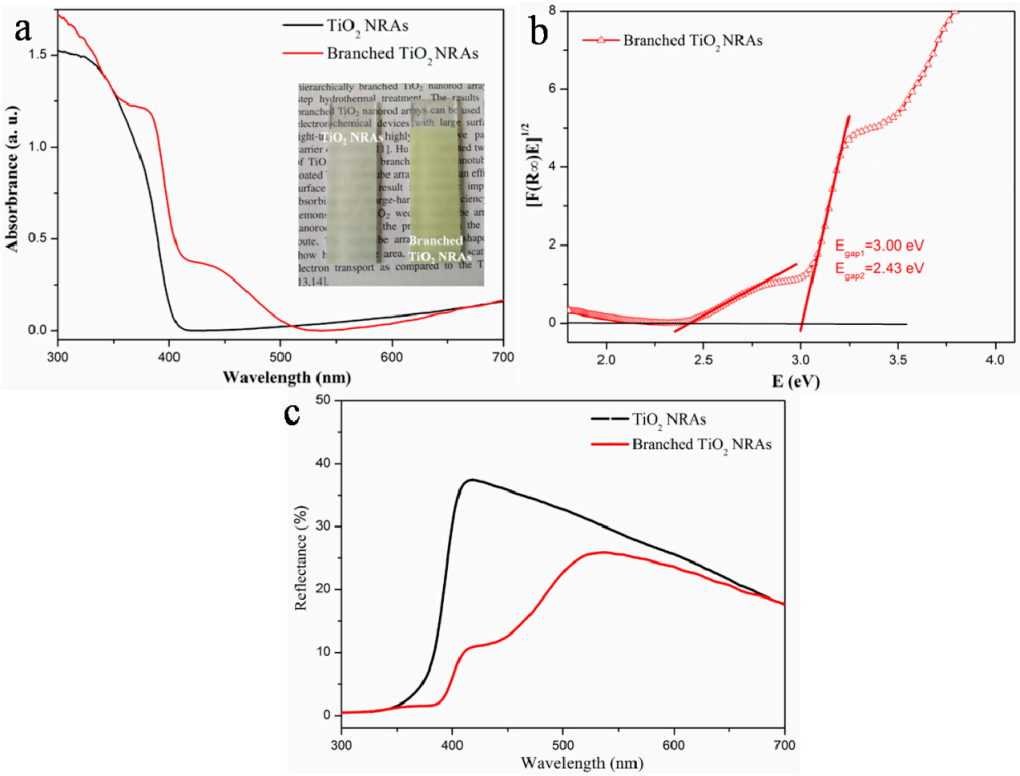

Figure 5. (**a**) Diffuse reflection absorption spectra, with an inset displaying the photo images of TiO_2 NRAs and branched NRAs; (**b**) transformed diffuse reflection absorption spectra of the branched NRAs and (**c**) diffuse reflection spectra of the TiO_2 NRAs and branched NRAs.

Figure 6a shows the linear sweep voltammpgrams curves of pure TiO_2 NRAs and branched TiO_2 NRAs under AM1.5G simulated sunlight. These results clearly showed that the photocurrent of branched TiO_2 NRAs was much higher than that of the pure TiO_2 NRAs film under visible-light illumination. The higher photocurrent indicated a higher efficiency in the separation of photon-generated electrons and holes, which resulted in a better PEC activity. Figure 6b shows the photocurrent response of TiO_2 NRAs and branched NRAs under pulsed visible-light irradiation at zero bias. TiO_2 NRAs and branched NRAs both exhibited the quick response to the switching of incident light, indicating a quick transfer of photogenerated electrons from the nanorod to the substrate [33]. This showed that the branched TiO_2 NRAs had the same high electron transport efficiency as pure TiO_2 NRAs. This conclusion was further confirmed by EIS spectroscopy (Figure 6c), as the exhibited large semicircle corresponds to the resistances of the TiO_2/FTO and TiO_2/electrolyte interfaces [34]. The diameter of the large semicircle measured for the cell using branched TiO_2 NRAs as the photoanode was only slightly larger than that for the cell using pure TiO_2 NRAs as the photoanode, suggesting that branched TiO_2 NRAs still exhibit better electron transport properties and lower series resistances [35].

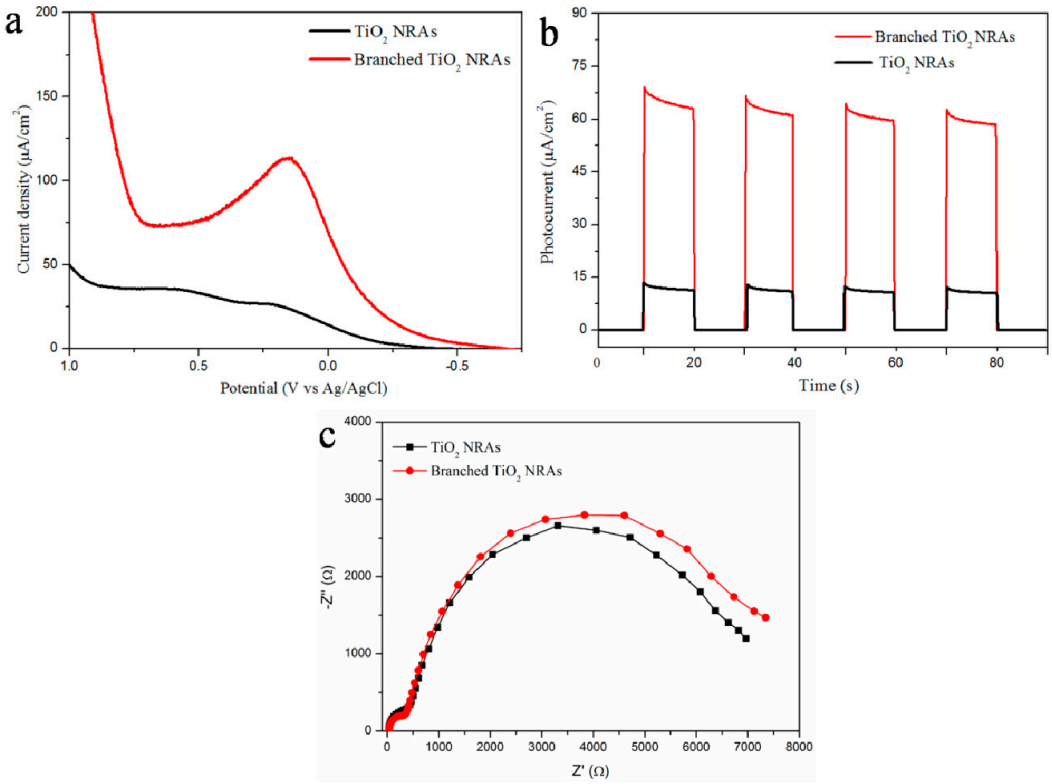

Figure 6. (**a**) Current-density versus voltage (*J*-*V*) curves and (**b**) photocurrent density response of TiO_2 NRAs and branched NRAs; (**c**) Nyquist plots of TiO_2 NRAs and branched NRAs based cells.

4. Conclusions

In summary, Ti^{3+} self-doped branched TiO_2 NRAs with visible light absorption were successfully prepared by combining a hydrothermal method with magnetron sputtering technology. Using TiO_2 NPs on the nanorods as seeds, the tree-like branched TiO_2 NRAs can be easily formed. The Ti^{3+} defects and oxygen vacancies in TiO_2 NPs and nanobranches expanded the absorption range of the TiO_2 NRAs to visible light region. Based on the larger surface area, the expanded optical absorption range, and the better carrier transport properties, branched TiO_2 NRAs exhibit better PEC activity than pure TiO_2 NRAs, which makes them promising candidates for applications in PEC, photovoltaic, and photocatalytic devices.

Author Contributions: Data curation, X.W. and Q.T.; investigation, X.W. and J.Y.; methodology, J.W. and J.Y.; project administration, J.W.; resources, Q.T.; supervision, G.L., S.Q. and Z.Z.; writing of the original draft, J.W.; writing of review and editing, G.L.

Funding: This research was funded by the National Natural Science Foundation of China (No. 51302075), Hubei Provincial Collaborative Innovation Center for Optoelectronics and Hubei Superior and Distinctive Discipline Group of "Mechatronics and Automobiles" (No. XKQ2018001).

Conflicts of Interest: The authors declare no conflicts of interest.

References

1. Wang, G.M.; Wang, H.Y.; Ling, Y.C.; Tang, Y.C.; Yang, X.Y.; Fitzmorris, R.C.; Wang, C.C.; Zhang, J.Z.; Li, Y. Hydrogen-treated TiO_2 nanowire arrays for photoelectrochemical water splitting. *Nano Lett.* **2011**, *11*, 3026–3033. [CrossRef] [PubMed]
2. Zhang, H.; Chen, Z.J.; Song, Y.; Yin, M.; Li, D.D.; Zhu, X.F.; Chen, X.Y.; Chang, P.C.; Lu, L.F. Fabrication and supercapacitive performance of long anodic TiO_2 nantotube arrays using constant current anodization. *Electrochem. Commun.* **2016**, *68*, 23–27. [CrossRef]

3. Wang, X.L.; Zhang, Z.L.; Qin, J.Q.; Shi, W.J.; Liu, T.F.; Gao, H.P.; Mao, Y.L. Enhanced photovoltaic performance of perovskite solar cells based on Er-Yb co-doped TiO_2 nanorod arrays. *Electrochim. Acta* **2017**, *245*, 839–845. [CrossRef]
4. Verghese, O.K.; Paulose, M.; Grimes, C.A. Long vertically aligned titania nanotubes on transparent conductive oxide for highly efficient solar cells. *Nat. Nanotechnol.* **2009**, *4*, 592–597. [CrossRef] [PubMed]
5. Xu, C.; Shin, P.H.; Cao, L.; Wu, J.; Gao, D. Ordered TiO_2 nanotube arrays on transparent conductive oxide for dye-sensitized solar cells. *Chem. Mater.* **2010**, *22*, 143–148. [CrossRef]
6. Wang, H.; Guo, Z.G.; Wang, S.M.; Liu, W.M. One-dimensional titania nanostructures: Synthseis and application in dye-sensitized solar cells. *Thin Solid Films* **2014**, *558*, 1–19. [CrossRef]
7. Liu, B.; Aydil, E.S. Growth of oriented single-crystalline rutile TiO_2 nanorods on transparent conducting substrates for dyesensitized solar cells. *J. Am. Chem. Soc.* **2009**, *131*, 3985–3990. [CrossRef] [PubMed]
8. Zhang, S.S.; Zhang, S.Q.; Peng, B.Y.; Wang, H.J.; Yu, H.; Wang, H.H.; Peng, F. High performance hydrogenated TiO_2 nanorod arrays as a photoelectrochemical sensor for organic compounds under visible light. *Electrochem. Commun.* **2014**, *40*, 24–27. [CrossRef]
9. Oh, J.K.; Lee, J.K.; Kim, H.S.; Han, S.B.; Park, K.W. TiO_2 branched nanostructure electrodes synthesized by seeding method for dye-sensitized solar cells. *Chem. Mater.* **2010**, *22*, 1114–1118. [CrossRef]
10. Cho, I.S.; Chen, Z.B.; Forman, A.J.; Kim, D.R.; Rao, P.M.; Jaramillo, T.F.; Zheng, X.L. Branched TiO_2 nanorods for photoelectrochemical hydrogen production. *Nano Lett.* **2011**, *11*, 4978–4984. [CrossRef] [PubMed]
11. Wang, H.; Bai, Y.S.; Wu, Q.; Zhou, W.; Zhang, H.; Li, J.H.; Guo, L. Rutile TiO_2 nano-branched arrays on FTO for dye-sensitized solar cells. *Phys. Chem. Chem. Phys.* **2011**, *13*, 7008–7013. [CrossRef] [PubMed]
12. Yang, J.S.; Liao, W.P.; Wu, J.J. Morphology and interfacial energetic controls for hierarchical anatase/rutile TiO_2 nanostructured array for efficient photoelectrochemical water splitting. *ACS Appl. Mater. Interfaces* **2013**, *5*, 7425–7431. [CrossRef] [PubMed]
13. Li, Y.M.; Guo, Y.; Li, Y.H.; Zhou, X.F. Fabrication of Cd-doped TiO_2 nanorod arrays and photovoltaic property in perovskite solar cell. *Electrochim. Acta* **2016**, *200*, 29–36. [CrossRef]
14. Lv, M.Q.; Zheng, D.J.; Ye, M.D.; Xiao, J.; Guo, W.X.; Lai, Y.K.; Sun, L.; Lin, C.J.; Zuo, J. Optimized porous rutile TiO_2 nanorod arrays for enhancing the efficiency of dye-sensitized solar cells. *Energy Environ. Sci.* **2013**, *6*, 1615–1622. [CrossRef]
15. Bang, J.H.; Kamat, P. Solar cells by design: Photoelectrochemistry of TiO_2 nanorod arrays decorated with CdSe. *Adv. Funct. Mater.* **2010**, *20*, 1970–1976. [CrossRef]
16. Hu, A.; Wang, J.Y.; Qu, S.H.; Zhong, Z.C.; Wang, S.; Liang, G.J. Hydrothermal growth of branched hierarchical TiO_2 nanorod arrays for application in dye-sensitized solar cells. *J. Mater. Sci. Mater. Electron.* **2017**, *28*, 3415–3422. [CrossRef]
17. Wang, J.Y.; Qu, S.H.; Zhong, Z.C.; Wang, S.; Liu, K.; Hu, A.Z. Fabrication of TiO_2 nanoparticles/nanorod composite arrays via a two-step method for efficient dye-sensitized solar cells. *Prog. Nat. Sci. Mater. Int.* **2014**, *24*, 588–592. [CrossRef]
18. Huang, Q.L.; Zhou, G.; Fang, L.; Hu, L.P.; Wang, Z.S. TiO_2 nanorod arrays grown from a mixed acid medium for efficient dye-sensitized solar cells. *Energy Environ. Sci.* **2011**, *4*, 2145–2151. [CrossRef]
19. Li, K.; Huang, Z.Y.; Zeng, Z.Q.; Huang, B.B.; Gao, S.M.; Lu, J. Synergetic effect of Ti^{3+} and oxygen doping on enhancing photoelectrochemical and photocatalytic properties of TiO_2/g-C_3N_4 heterojunctions. *ACS Appl. Mater. Interfaces* **2017**, *9*, 11577–11586. [CrossRef] [PubMed]
20. Liu, M.; Qiu, X.Q.; Miyauchi, M.; Hashimoto, K. Cu (II) oxide amorphous nanoclusters grafted Ti^{3+} self-doped TiO_2: An efficient visible light photocatalyst. *Chem. Mater.* **2011**, *23*, 5282–5286. [CrossRef]
21. Kong, L.N.; Wang, C.H.; Zheng, H.; Zhang, X.T.; Liu, Y.C. Defect-induced yellow color in Nb-doped TiO_2 and its impact on visible-light photocatalysis. *J. Phys. Chem. C* **2015**, *119*, 16623–16632. [CrossRef]
22. Zhang, Y.; Xing, Z.P.; Liu, X.F.; Li, Z.Z.; Wu, X.Y.; Jiang, J.J.; Ki, M.; Zhu, Q.; Zhou, W. Ti^{3+} self-doped blue TiO_2 (B) single-crystalline nanorods for efficient solar-driven photocatalytic performance. *ACS Appl. Mater. Interfaces* **2016**, *8*, 26851–26859. [CrossRef] [PubMed]
23. Zuo, F.; Wang, L.; Wu, T.; Zhang, Z.Y.; Borchardt, D.; Feng, P.Y. Self-doped Ti^{3+} enhanced photocatalyst for hydrogen production under visible light. *J. Am. Chem. Soc.* **2010**, *132*, 11856–11857. [CrossRef] [PubMed]
24. Fu, R.R.; Wang, Q.Y.; Gao, S.M.; Wang, Z.Y.; Huang, B.B.; Dai, Y.; Lu, J. Effect of different processes and Ti/Zn molar ratios on the structure, morphology, and enhanced photoelectrochemical and photocatalytic performance of Ti^{3+} self-doped titanium–zinc hybrid oxides. *J. Power Sources* **2015**, *285*, 449–459. [CrossRef]

25. Su, J.; Zou, X.X.; Chen, J.S. Self-modification of titanium dioxide materials by Ti^{3+} and/or oxygen vacancies: new insights into defect chemistry of metal oxides. *RSC Adv.* **2014**, *4*, 13979–13988. [CrossRef]
26. Chen, X.B.; Liu, L.; Huang, F.Q. Black titanium dioxide (TiO_2) nanomaterials. *Chem. Soc. Rev.* **2015**, *44*, 1861–1885. [CrossRef] [PubMed]
27. Chinnamuthu, P.; Mondal, A.; Singh, N.K.; Dhar, J.C.; Chattopadhyay, K.K.; Bhattacharya, S. Band gap enhancement of glancing angel deposited TiO_2 nanowire array. *J. Appl. Phys.* **2012**, *112*, 054315. [CrossRef]
28. Bu, J.; Fang, J.; Leow, W.R.; Zheng, K.H.; Chen, X.D. Single-crystalline rutile TiO_2 nano-flower hierarchical structure for enhanced photocatalytic selective oxidation from amine to imine. *RSC Adv.* **2015**, *5*, 103895–103900. [CrossRef]
29. Diedenhofen, S.L.; Vecchi, G.; Algra, R.E.; Hartsuiker, A.; Muskens, O.L.; Immink, G.; Bakkers, E.; Vos, W.L.; Rivas, J.G. Broad-band and omnidirectional antireflection coatings based on semiconductor nanorods. *Adv. Mater.* **2009**, *21*, 973–978. [CrossRef]
30. Zhang, S.S.; Wang, X.J.; Hu, J.Y.; Xie, Z.K.; Lei, H.G.; Peng, F. Design of two kinds of branched TiO_2 nanoarray photoanodes and their comparison of photoelectrochemical performances. *Electrochim. Acta* **2017**, *25*, 368–373. [CrossRef]
31. Liu, J.; Yu, X.L.; Liu, Q.Y.; Liu, R.J.; Shang, X.K.; Zhang, S.S.; Li, W.H.; Zheng, W.Q.; Zhang, G.J.; Cao, H.B.; Gu, Z.J. Surface-phase junctions of branched TiO_2 nanorod arrays for efficient photoelectrochemical water splitting. *Appl. Catal. B Environ.* **2014**, *158–159*, 296–300. [CrossRef]
32. Wang, L.Y.; Daoud, W.A. BiOI/TiO_2-nanorod array heterojunction solar cell: Growth, charge transport kinetics and photoelectrochemical properties. *Appl. Surf. Sci.* **2015**, *324*, 532–537. [CrossRef]
33. Wang, P.; Zhang, Y.; Su, L.; Gao, W.Z.; Zhang, B.L.; Chu, H.R. Photoelectrochemical properties of CdS/CdSe sensitized TiO_2 nanocable arrays. *Electrochim. Acta* **2015**, *165*, 110–115. [CrossRef]
34. Lee, K.M.; Suryanarayanan, V.; Ho, K.C. A study on the electron transport properties of TiO_2 electrodes in sye-snesitized solar cells. *Sol. Energy Mater. Sol. Cells* **2007**, *91*, 1416–1420. [CrossRef]
35. Neto, S.Y.; Luz, R.C.S.; Damos, F.S. Visible LED light photoelectrochemical sensor for detection of L-dopa based on oxygen reduction on TiO_2 sensitzied with iron phthalocyanine. *Electrochem. Commun.* **2016**, *62*, 1–4. [CrossRef]